INTERNATIONAL JOURNAL OF PRECISION ENGINEERING AND MANUFACTURING-GREEN TECHNOLOGY Vol. 5, No. 2, pp. 219-230 APRIL 2018 / 219

REGULAR PAPER

DOI: 10.1007/s40684-018-0022-9
ISSN 2288-6206 (Print) / 2198-0810 (Online)

Experimental Investigation and Mechanism Analysis of Tungsten Disulfide Soft Coated Micro-Nano Textured Self-Lubricating Dry Cutting Tools

Yunsong Lian[1,#], Huifeng Chen[1], Chenliang Mu[1], Jianxin Deng[2], and Shuting Lei[3]

1 Department of Mechanical and Electrical Engineering, Xiamen University, Xiamen, Fujian Province, 361005, PR China
2 School of Mechanical Engineering, Shandong University, Jinan, Shandong Province, 250061, PR China
3 Department of Industrial and Manufacturing Systems Engineering, Kansas State University, Manhattan, 66506, KS, USA
Corresponding Author / E-mail: lianys@xmu.edu.cn, TEL: +86-15659837368
ORCID: 0000-0001-5489-7018

KEYWORDS: Dry cutting tool, Self-lubricating mechanism, Micro-Nano texture, WS_2 soft coating, Tool life

A new dry cutting tool named WS_2 soft coated Micro-Nano textured self-lubricating dry cutting tool (WTT tool) is developed and tested. Dry turning tests have been carried out on 45# quenched and tempered steel with a WTT tool and three other types of alternative tools. The machining performance was assessed in terms of the cutting forces, cutting temperature, friction coefficient at the tool-chip interface, chip deformation, tool wear, and the surface roughness of the machined workpiece. The results show that the WTT tool has the best cutting performance among all the tools tested under the same cutting conditions. Through theoretical analysis and experimental results, the mechanisms of the WTT tool in improving cutting performance were put forward. Meanwhile, the effect of Micro-Nano texture and WS_2 soft coating on the cutting forces and the cutting temperature is analyzed. It can be concluded that the WTT tool can effectively improve the anti-adhesion and wear-resistance properties and increase the tool life.

Manuscript received: May 16, 2017 / Revised: November 22, 2017 / Accepted: December 11, 2017

1. Introduction

Severe friction occurs in metal cutting operations when the tool contacts with a workpiece both by the rake face and tool flank. Moreover, the high temperature involved in cutting processes increases crater wear and therefore results in a shorter tool life.[1,2] In order to alleviate and reduce the severe friction and wear on tools is by using cutting fluids during the process. The cutting fluid provides lubricating and cooling functions which can assist in the reduction of the cutting temperature and friction forces. This results in a substantial increase of tool life and reduction of the workpiece surface roughness. However, the lubrication effectiveness of cutting fluids reduces with its difficult infiltration into the tool-chip intimate interface in high speed machining. Besides that, many of the fluids contain environmentally harmful constituents, which are difficult to dispose of and also expensive to recycle.[3] Due to the negative effects associated with the cutting fluids, research on dry metal machining (without cutting fluids) attracts much attention for its active role in reducing environmental pollution and production costs.

On the other hand, the friction and adhesion between the chip and tool are higher in dry machining. This causes higher temperatures, higher wear rates and, finally, a shorter tool life. To solve these problems, new cutting tools with reduced friction coefficient have been suggested. A spectrum of avenues, including developing advanced tool materials,[4-6] tool coating,[7,8] and lubricant addition,[9,10] was attempted in the exploitation of dry cutting tools. Deng et al.[10] reported an Al_2O_3/TiC-based ceramic cutting tool with the addition of CaF_2 solid lubricant. It was discovered that the friction coefficient at the tool-chip interface in dry cutting with this ceramic tool can be reduced in comparison with the tool without a solid lubricant. This effect was attributed to the formation of the self-tribofilm.

According to the traditional tribological viewpoint, the milder tool wear could be obtained with smoother friction pairs. However, researches[11-14] have indicated that micro-textured surfaces which are non-smooth may have excellent performance in reducing friction and wear under certain conditions. Recently, a series of cutter designs with surface texturing has been reported.[15-20] For example, Sugihara et al.[18] found that a cutting tool with a Nano/Micro-textured surface made by means of femtosecond laser technology possessed antiadhesive effects

at the tool-chip interface. Koshy and Tovey[20] applied electrical discharge machining to generate an isotropic texture on the tool rake face. A significant reduction in feed and cutting forces ensued due to the said texturing.

The micro-textured self-lubricating tool for dry machining is known in a wide range of dry machining tools. The performance of dry cutting 45# steel by a kind of carbide tool with a textured rake face was reported.[21] In comparison to conventional tools, the application of the rake face textured tools can significantly reduce cutting forces and the cutting temperature. Nevertheless, we still found some problems with the micro-textured self-lubricating tools. Firstly, it was difficult to fill the micron textures which were fabricated by a laser diode (LD) side-pumped solid-state laser with solid lubricant to prepare the micro-textured self-lubricating tools. Secondly, it caused more abrasive wear between the surface of the cutting tool and the workpiece because of the poor surface quality created by the LD side-pumped solid-state laser machining.

Surface coating is an effective method to resolve the difficulty in filling the textures with solid lubricant. There are some commonly used soft solid lubricants such as molybdenum disulfide (MoS_2), graphite (C), and boron nitride (BN). MoS_2 is a well-known lamellar solid lubricant with a hexagonal structure.[22] MoS_2 soft coating and its composite soft coating have been extensively used for the ultra-low friction of MoS_2 soft coatings. However, the weakness of MoS_2 soft coatings is also apparent. When the temperature reaches 400°C, MoS_2 soft coating begins to be oxidized to form MoO_3 which sharply decreases the lubricity of the MoS_2 soft coating.[23] Moreover, the MoS_2 soft coating is very sensitive to environmental humidity. When the environmental humidity changes from 10 to 90%, the friction coefficient of the MoS_2 soft coating doubles.[24] Therefore, it is necessary to study a new kind of soft coating.

Tungsten disulfide (WS_2) is an excellent lamellar solid lubricant. It has physical (prevents adhesion), chemical (high oxidation resistance) and microstructural (lamellar structure with ultralow shear strength) influence on a tribological contact of the working surfaces. The mechanism behind its effective lubricating performance is attributed to easy shearing along the basal planes of the hexagonal crystalline structures named II texture.[25,26] Recently, WS_2 soft coating's low friction has attracted growing attention for a variety of applications.[27-30] In applying WS_2 soft coating to the Micro-Nano textured tools with its excellent lubricity, it will form a continuous solid lubricating layer on the surface of the Micro-Nano textured tools to reduce friction, the cutting forces, and the cutting temperature.

A new dry cutting tool named WS_2 soft coated Micro-Nano textured self-lubricating dry cutting tool was fabricated for better performance in dry machining. In this paper, we describe the dry turning tests on 45# quenched and tempered steel with WS_2 soft coated Micro-Nano textured self-lubricating dry cutting tool and three other kinds of alternative tools. An assessment of the machining performance was based on the cutting forces, cutting temperature, friction coefficient at the tool-chip interface, tool wear and the surface roughness. Through the theoretical analysis and experimental results, the mechanisms of improving cutting performance using the WS_2 soft coated Micro-Nano textured self-lubricating dry cutting tool were put forward.

2. Experimental Details

2.1 Preparation of WS_2 Soft Coated Micro-Nano Textured Self-lubricating Dry Cutting Tool

The WS_2 soft coated Micro-Nano textured self-lubricating dry cutting tool was fabricated in two steps. Firstly, the Micro-Nano textures were processed both on the tool-chip interface of the rake face and the tool-workpiece interface of the flank face of the uncoated YS8 (WC+TiC+Co) cemented carbide cutting inserts by femtosecond laser micromachining technology. Secondly, the WS_2 soft coating was deposited on the Micro-Nano textured tool by medium-frequency magnetron sputtering, multi-arc ion plating, and ion beam assisted deposition technique. Fig. 1 shows the surface topography of the WS_2 soft coated Micro-Nano textured self-lubricating dry cutting tool. The texture period, texture depth, and texture width of the WS_2 soft coated Micro-Nano textures are characterized by scanning probe microscope (SPM). Fig. 2 indicates that the SPM and cross sectional profile of WS_2 soft coated Micro-Nano textures. The texture period (673 nm), texture depth (121 nm), and texture width (334 nm) of the WS_2 soft coated Micro-Nano textures are obtained after five measurements.

2.2 Cutting Tests

Turning tests were carried out on a CA6140 lathe equipped with a commercial tool holder with the following geometry: rake angle, γ_o = -5°; clearance angle, α_o = 5°; inclination angle, λ_s = 0°; side cutting edge angle, K_r = 45°; nose radius, r_ε = 0.5 mm. Four kinds of cutting tools were used: conventional YS8 cemented carbide cutting tool (without textured and coated) named CT tool, WS_2 soft coated tool (without textured) named WCT tool, Micro-Nano textured tool (without coated) named TT tool, and WS_2 soft coated Micro-Nano

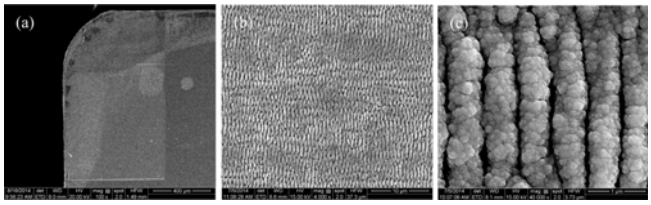

Fig. 1 Surface topography of the WS2 soft coated Micro-Nano textured self-lubricating dry cutting tool: (a) ×100 SEM photo of tool nose, (b) ×4000 SEM photo of WS_2 soft coated Micro-Nano textures, and (c) ×40000 SEM photo of WS_2 soft coated Micro-Nano textures

Table 1 Four kinds of cutting tools used in the turning tests

Cutting tool	Micro-Nano textured	Soft coated	Conventional cutting tool	Schematic diagram
CT tool			√	
WCT tool		√	√	
TT tool	√		√	
WTT tool	√	√	√	

textured self-lubricating dry cutting tool named WTT tool, as shown in Table 1. The geometry of the inserts was of ISO SNGN150608. The workpiece material used was 45# quenched and tempered steel (Chinese standard GB99-88) in the form of a round bar (HRC 20, Φ 100 mm). No cutting fluid was used in the machining processes. All the tests were carried out with the following parameters: depth of cut, a_p = 0.3 mm; feed rate, f = 0.1 mm/r; cutting speed, v = 50~250 m/min.

Under the cutting conditions, each test was replicated three times. Cutting forces were measured by a Kistler piezoelectric quartz dynamometer (type 9275A) linked via charge amplifier to a data acquisition system which consists of an A/D converter and a signal analyzer software on PC. The average cutting temperature of the tool rake face was measured by a TH5104R infrared thermal imaging system. The surface roughness of the machined workpiece was measured by a Time (type TR200) handheld roughness tester. During the cutting tests, type JCD-2 portable digital microscope was used to observe the wear condition of cutting tools. SEM was used to examine the morphology of the worn region of the cutting tool after the cutting tests. The chemical composition at the wear track was identified by the energy dispersive X-ray spectroscopy (EDX).

3. Results and Discussion

3.1 Cutting Forces

Fig. 3 illustrates three cutting force components (main cutting force F_z, radial thrust force F_y, and axial thrust force F_x) at different cutting speeds with CT, WCT, TT, and WTT tools in dry cutting. It can be seen from Fig. 3 that the three cutting force components of the four tools first increase and then decrease with the increase of cutting speed. Meanwhile, three cutting force components of WCT, TT, and WTT tools are reduced by 9~31%, 8~18%, and 10~44%, respectively, when compared with those of the CT tool. In addition, WTT tool shows the smallest cutting forces among all the tools tested under the same cutting conditions, especially in relatively high-speed conditions.

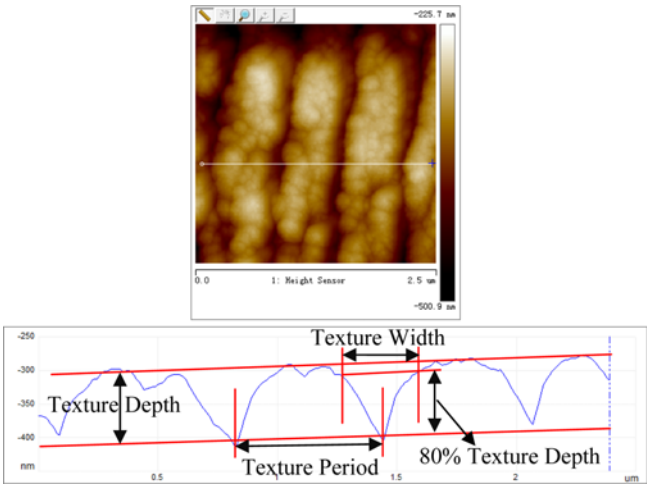

Fig. 2 SPM and cross sectional profile of the WS_2 soft coated Micro-Nano textures

3.2 Cutting Temperature

Fig. 4 shows the temperature distribution of the tool nose of the WTT tool measured by infrared thermal imaging system in dry cutting (v = 250 m/min, f = 0.1 mm/r, a_p = 0.3 mm). It is important to note that the highest temperature at tool nose position in this measurement is 382.3°C. The temperature distribution was measured at 5-s intervals in the cutting process. The average values of the highest temperature at the tool nose position in each measurement in three repeated experiments are used to compare.

Fig. 5 illustrates the cutting temperature of the CT, WCT, TT, and WTT tools at different cutting speeds. It is evident that the cutting temperature increases with increasing cutting speed. From this figure, it is found that cutting temperature of WCT, TT, and

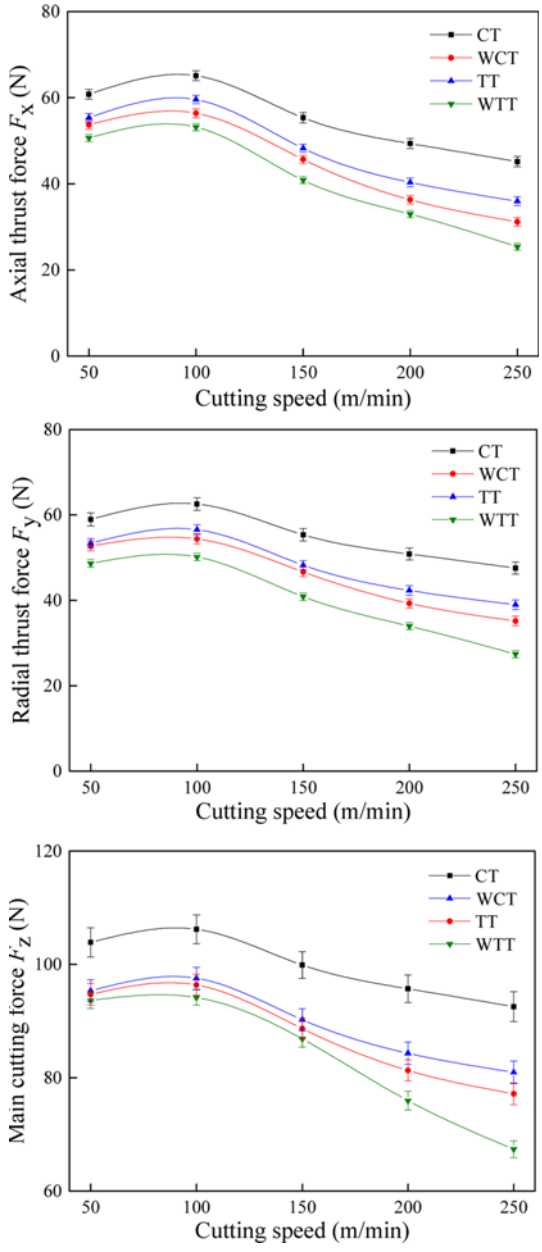

Fig. 3 Cutting forces of CT, WCT, TT, and WTT tools at different cutting speeds: (a) axial thrust force F_x, (b) radial thrust force F_y, and (c) main cutting force F_z (a_p = 0.3 mm, f = 0.1 mm/r)

WTT tools are reduced by 10~12%, 8~9%, and 12~16%, respectively, when compared with that of the CT tool. Among all the tools tested, the WTT tool shows the smallest cutting temperature under the same cutting conditions, in particular in relatively high-speed conditions. The advantage of WTT tool in cutting forces and cutting temperature is obvious at relatively high-speed and high-temperature conditions. This could be potentially as a result of the ultra-low friction coefficient, high temperature resistance, and the high oxidation resistance of WS_2 soft coating which is not sensitive to high cutting temperature and high cutting speed can significantly improve the severe dry cutting environment. Besides, Micro-Nano textures in the WTT tool plays a role of storing WS_2 soft coating which results in the extension of WS_2 soft coating life during the cutting process. However, due to without Micro-Nano textures, the WS_2 soft coating on the WCT tool wears much faster which leads to the rise of cutting temperature, especially in relatively high-speed conditions.

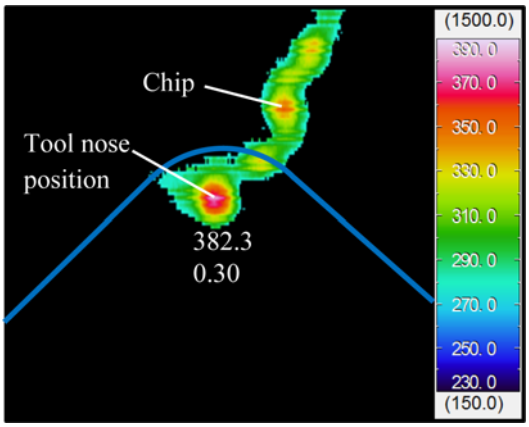

Fig. 4 Cutting temperature distribution of tool nose of the WTT tool measured by infrared thermal imaging system in dry cutting (v = 250 m/min, f = 0.1 mm/r, a_p = 0.3 mm)

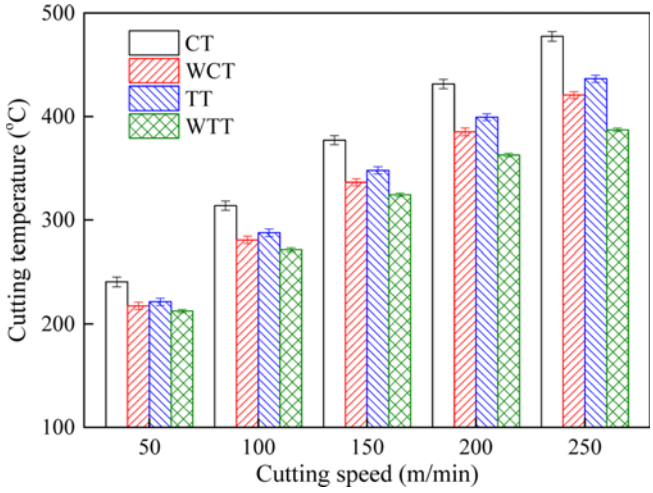

Fig. 5 Cutting temperature at the tool nose of the CT, WCT, TT, and WTT tools at different cutting speeds (a_p = 0.3 mm, f = 0.1 mm/r)

3.3 Average Friction Coefficient at the Tool-Chip Interface

Based on the metal cutting principle, during the cutting process, the average friction coefficient at the tool-chip interface could be calculated using the following formula:[31]

$$\mu = \tan\beta = \tan\left(\gamma_o + \arctan\frac{F_y}{F_z}\right) \quad (1)$$

where β is the friction angle, γ_o is the rake angle, F_y is the radial thrust force, and F_z is the main cutting force.

Fig. 6 illustrates the average friction coefficient at the tool-chip interface of the CT, WCT, TT, and WTT tools as a function of cutting speeds in dry cutting. It is indicated that the friction coefficients follow the same trend as the cutting forces whereby it increases first then decreases. From this figure, it is found that the average friction coefficient at the tool-chip interface of the WCT, TT, and WTT tools are reduced by 2~13%, 2~7%, and 10~25%, respectively, in comparison to the CT tool. Furthermore, the WTT tool has the smallest average friction coefficient at the tool-chip interface among all the tools tested.

3.4 Chip Deformation

The chips produced by the cutting of metal are usually thicker and

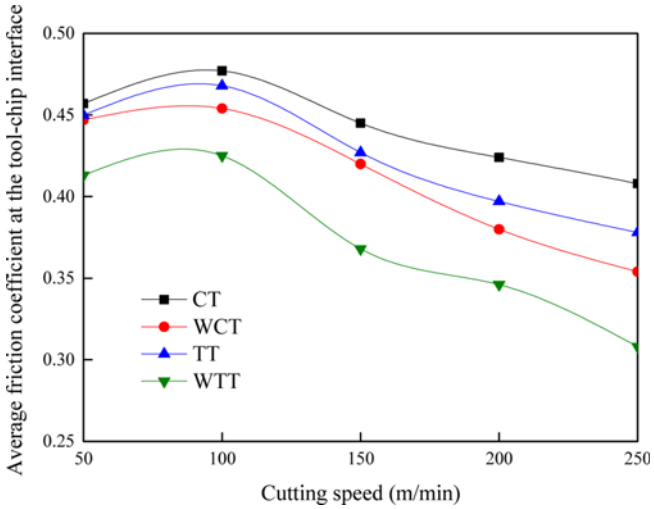

Fig. 6 Average friction coefficient at the tool-chip interface of the CT, WCT, TT, and WTT tools at different cutting speeds (a_p = 0.3 mm, f = 0.1 mm/r)

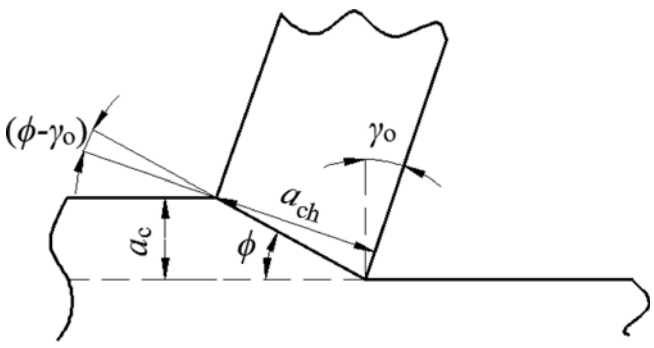

Fig. 7 Sketch of chip deformation during cutting

shorter than local dimensions of the material before cutting. In most cases, the deformation of the chip is approximately two-dimensional. Along with this, the change of cutting width and volume can be ignored. So, it can be assumed that the chip volume is the same before and after cutting. Based on the metal cutting principle, during the cutting process, the chip deformation can be calculated as the following formula:

$$\xi = \frac{a_{ch}}{a_c} \tag{2}$$

where ξ is the chip deformation coefficient which directly reflects the deformation degree of the chip, a_c is the uncut chip thickness, and a_{ch} is the chip thickness, as shown in Fig. 7.

Fig. 7 shows that the relationship between shear angle ϕ and chip deformation coefficient ξ can be calculated based on the following formula:

$$\tan\phi = \frac{\cos\gamma_o}{\xi - \sin\gamma_o} \tag{3}$$

where γ_o is the rake angle of cutting tool.

The uncut chip thickness a_c can be calculated based on the following formula:

$$a_c = f \sin K_r \tag{4}$$

where f is the feed rate and K_r is the side cutting edge angle.

According to Eqs. 2 and 4, the chip deformation coefficient ξ can be obtained by measuring the chip thickness a_{ch} (f = 0.1 mm/r, K_r = 45°). Fig. 8 illustrates the chip deformation coefficient of the CT, WCT, TT, and WTT tools at different cutting speeds. It can be seen from Fig. 8 that the chip deformation coefficient decreases with increasing cutting speed. The reduction of the chip deformation coefficient means the decrease of the chip deformation degree which can lead to a smaller cutting force and a lower cutting temperature. Meanwhile, the chip deformation coefficient of WTT tool is the smallest among all the tools tested under the same cutting speed. Besides, the chip deformation coefficient of WCT, TT, and WTT tools are reduced by 6~11%, 9~16%,

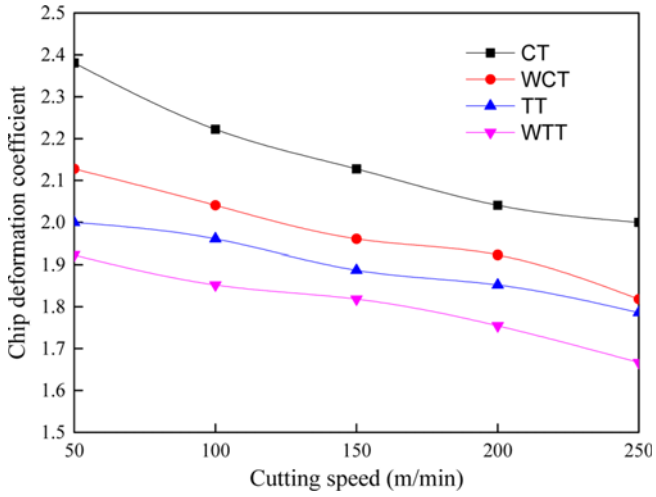

Fig. 8 Chip deformation coefficient of the CT, WCT, TT, and WTT tools at different cutting speeds (a_p = 0.3 mm, f = 0.1 mm/r)

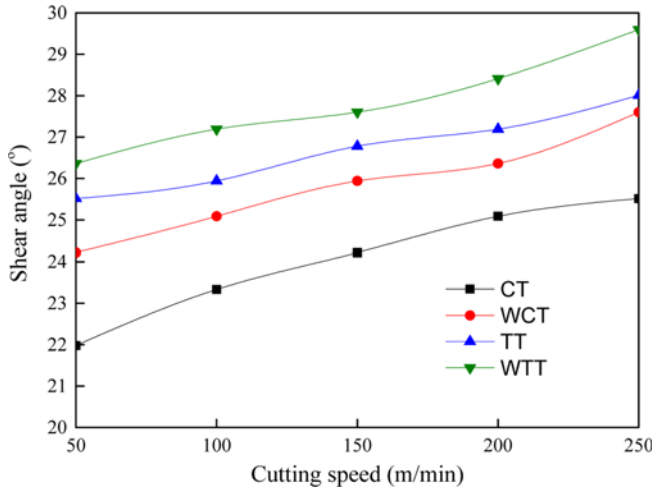

Fig. 9 Shear angle of the CT, WCT, TT, and WTT tools at different cutting speeds (a_p = 0.3 mm, f = 0.1 mm/r)

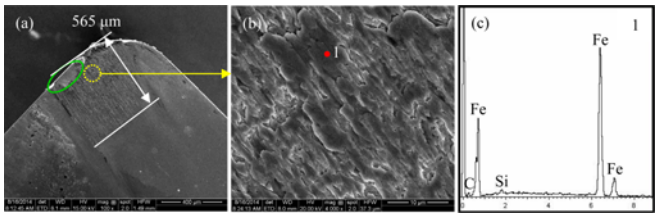

Fig. 10 SEM images of the worn rake face of the CT tool after 4-min dry cutting 45# quenched and tempered steel and the EDX chemical composition analysis in the selected areas (v = 150 m/min, f = 0.1 mm/r, a_p = 0.3 mm)

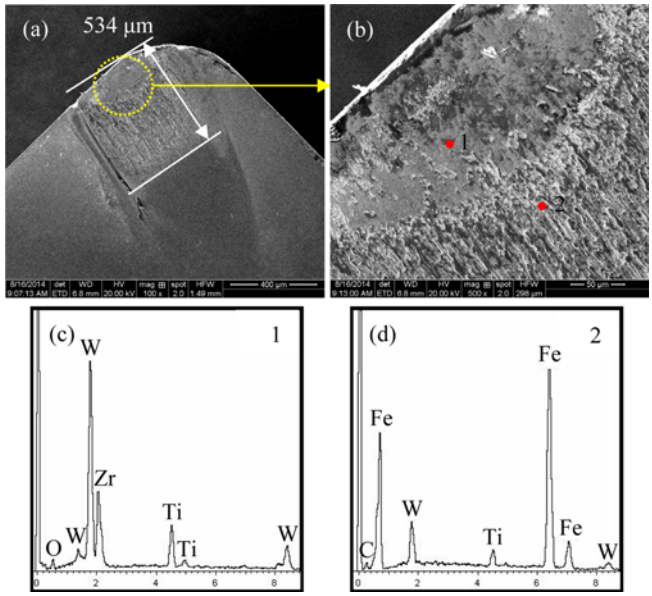

Fig. 11 SEM images of the worn rake face of the WCT tool after 4-min dry cutting 45# quenched and tempered steel and the EDX chemical composition analysis in the selected areas (v = 150 m/min, f = 0.1 mm/r, a_p = 0.3 mm)

and 14~19%, respectively, when compared with that of the CT tool.

The shear angle ϕ can be obtained per Eq. 3 and the chip deformation coefficient (rake angle γ_o = -5°). Fig. 9 illustrates the shear angle of the CT, WCT, TT, and WTT tools at different cutting speeds. It can be seen from Fig. 9 that the shear angle constantly increases with the increase of cutting speed. Meanwhile, the shear angle of WTT tool is the largest among all the tools tested under the same cutting speed. Besides, the shear angle of WCT, TT, and WTT tools are increased by 5~10%, 8~16%, and 13~20%, respectively, when compared with that of the CT tool.

3.5 Tool Wear

Figs. 10-13 show the SEM images of the worn rake face of the CT, WCT, TT, and WTT tools after 4-min dry cutting 45# quenched and tempered steel and the EDX chemical composition analysis in the selected areas (v = 150 m/min, f = 0.1 mm/r, a_p = 0.3 mm). The nominal tool-chip contact length of the cutting tool can be measured by observing the chip flow direction on the rake face of the cutting tool. The nominal tool-chip contact length of the CT, WCT, TT, and WTT tools are 565 μm, 534 μm, 544 μm, and 497 μm, respectively. It is found that the nominal tool-chip contact length of the WTT tool is the shortest among all.

Fig. 10 indicates that the adhesive wear is relatively intense on the rake face of the CT tool. It can be seen from Fig. 10(a) that a large area near the cutting edge was peeled off, as shown in the green ellipse. This could be due to the formation of the built-up edge near the cutting edge and the built up edge peeled off during the cutting process. It can be seen from Figs. 10(b) and 10(c) that the tool-chip contact area on the rake face was covered with massive iron filings.

Fig. 11 shows that the adhesive wear of the WCT tool is slighter than that of the CT tool, but the adhesive wear is still the major wear form on the rake face of the WCT tool. It can be seen from Figs. 11(b) and 11(d) that the tool-chip contact area on the rake face was covered with massive iron filings as well. However, the WS_2 soft coating was worn out (without S and Zr elements, Zr is the interlayer element). It can be seen from Figs. 11(b) and 11(c) that there is an area near the cutting edge without iron bonding. Meanwhile, interlayer Zr element was found and it showed that the WS_2 soft coating in this area was not completely worn out. The phenomenon of Fig. 11(b) is similar with Fig. 10. This could be due to the peeled off built up edge formed on the surface of the WS_2 soft coating which lead to a large area being exposed.

Fig. 12 shows that the wear condition of the TT tool is slighter than that of the WCT tool and the CT tool, but the rake face of the TT tool was also covered with some iron filings. It can be seen from Fig. 12(b) that some Micro-Nano textures still can be observed on the rake face of the TT tool (as shown in green circle), but not in the entire contact area. It can be established from the EDX chemical composition analysis that the vanishing Micro-Nano textures were covered over by scrap iron and not worn out. Besides, it can be seen from Fig. 12(a) that part area near the cutting edge was peeled off, as shown in the red ellipse. It may be because the built-up edge was formed near the cutting edge and the built-up edge was peeled off with tool materials in the cutting process.

Fig. 13 shows the SEM micrograph of the worn rake face of the WTT tool. It can be seen from Fig. 13(b) that the Micro-Nano textures can be observed clearly on the rake face of the WTT tool. Meanwhile, the surface of the Micro-Nano textures was found covered with a thin film. Through the EDX chemical composition analysis we can get that the main components of the thin film covered on the Micro-Nano textures are WS_2 soft coating with small amount of iron. The thin WS_2 lubricating film formed on the surface of the Micro-Nano textures can effectively reduce the tool-chip contact length and therefore improve the adhesion and wear condition on the rake face of the WTT tool. WTT tool shows the best anti-adhesion and wear-resistance properties on the rake face among all the tools tested under the same cutting conditions.

Figs. 14-17 show the SEM images of the worn flank face of the CT, WCT, TT, and WTT tools after 4-min dry cutting 45# quenched and tempered steel and the EDX chemical composition analysis in the selected areas (v = 150 m/min, f = 0.1 mm/r, a_p = 0.3 mm). The worn depth at the tool nose of the cutting tool can be measured from the

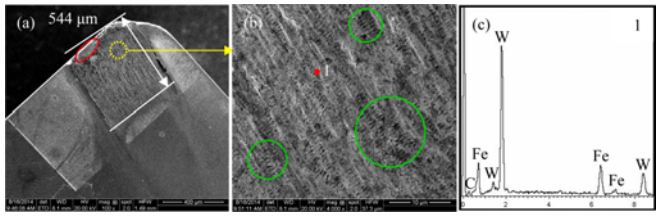

Fig. 12 SEM images of the worn rake face of the TT tool after 4-min dry cutting 45# quenched and tempered steel and the EDX chemical composition analysis in the selected areas (v = 150 m/min, f = 0.1 mm/r, a_p = 0.3 mm)

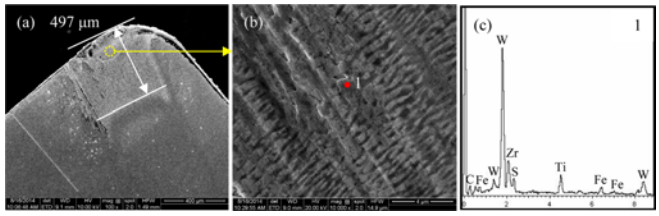

Fig. 13 SEM images of the worn rake face of the WTT tool after 4-min dry cutting 45# quenched and tempered steel and the EDX chemical composition analysis in the selected areas (v = 150 m/min, f = 0.1 mm/r, a_p = 0.3 mm)

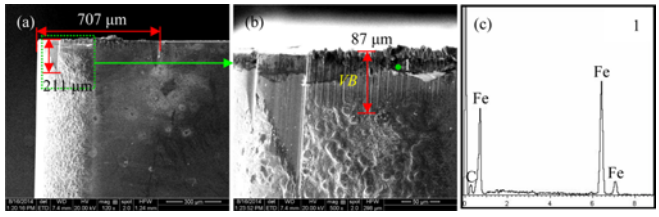

Fig. 14 SEM images of the worn flank face of the CT tool after 4-min dry cutting 45# quenched and tempered steel and the EDX chemical composition analysis in the selected areas (v = 150 m/min, f = 0.1 mm/r, a_p = 0.3 mm)

SEM images of the worn flank face of four tools. The worn depth at the tool nose of the CT, WCT, TT, and WTT tools are 211 μm, 206 μm, 201 μm, and 176 μm, respectively. It is found that the worn depth at the tool nose of the WTT tool is the shortest among all the tools tested. Moreover, the worn depth at the tool nose of the WCT, TT, and WTT tools are reduced by 2%, 5%, and 17%, respectively, when compared with that of the CT tool.

The worn width *VB* is usually used to measure the wear loss at the flank face of the tool, as shown in Panel b of Figs. 14-17. The worn width *VB* at the flank face of the CT, WCT, TT, and WTT tools are 87 μm, 73 μm, 72 μm, and 64 μm, respectively. Thus the worn width *VB* at the flank face of the WTT tool is the narrowest among all the tools tested. Furthermore, the worn width *VB* at the flank face of the WCT, TT, and WTT tools are decreased by 16%, 17%, and 26%, respectively, when compared with that of the CT tool.

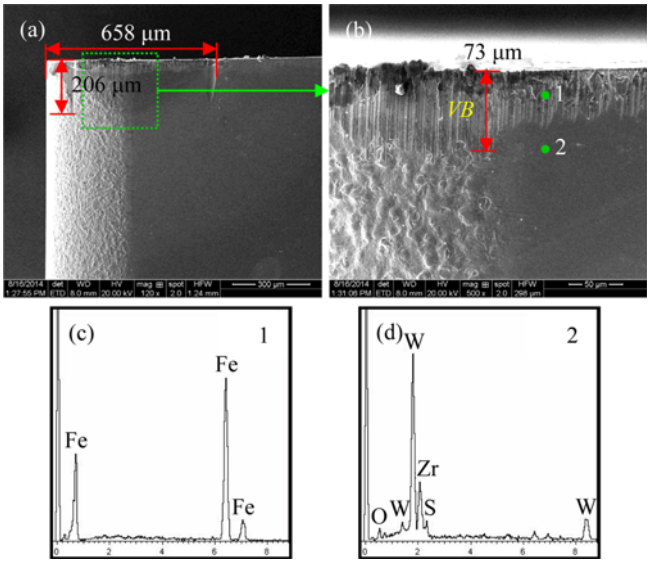

Fig. 15 SEM images of the worn flank face of the WCT tool after 4-min dry cutting 45# quenched and tempered steel and the EDX chemical composition analysis in the selected areas (v = 150 m/min, f = 0.1 mm/r, a_p = 0.3 mm)

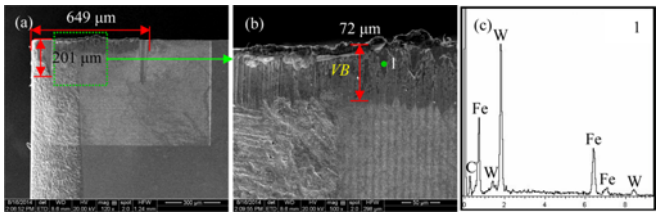

Fig. 16 SEM images of the worn flank face of the TT tool after 4-min dry cutting 45# quenched and tempered steel and the EDX chemical composition analysis in the selected areas (v = 150 m/min, f = 0.1 mm/r, a_p = 0.3 mm)

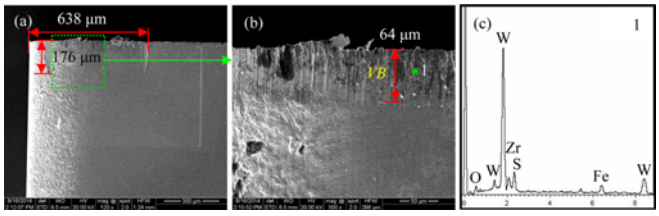

Fig. 17 SEM images of the worn flank face of the WTT tool after 4-min dry cutting 45# quenched and tempered steel and the EDX chemical composition analysis in the selected areas (v = 150 m/min, f = 0.1 mm/r, a_p = 0.3 mm)

Panels a in Figs. 14-17 show that the worn length at the flank face of the CT, WCT, TT, and WTT tools are 707 μm, 658 μm, 649 μm, and 638 μm, respectively. It is found that the worn length at the flank face of the WCT, TT, and WTT tools are decreased by 7%, 8%, and 10%, respectively, when compared with that of the CT tool.

Panels a and b in Fig. 14 show the SEM images of the worn flank face of the CT tool after 4-min dry cutting 45# quenched and tempered steel. It can be seen that the flank wear of the CT tool is relatively serious. The main wear forms of the CT tool are abrasive wear, corner wear, boundary wear, and adhesive wear. Through the EDX chemical composition analysis it is found that the wear area at the flank face near the main cutting edge of the CT tool was also covered with some iron filings.

Panels a and b in Fig. 15 show the SEM images of the worn flank face of the WCT tool after 4-min dry cutting 45# quenched and tempered steel. It can be seen that the wear condition of the WCT tool is slighter than that of the CT tool. However, the main wear forms of the WCT tool are still abrasive wear, corner wear, boundary wear, and adhesive wear. The EDX chemical composition analysis is shown that the wear area at the flank face near the main cutting edge of the WCT tool was covered with iron fillings. Meanwhile, the WS_2 soft coating at this wear area was worn out.

Panels a and b in Fig. 16 show the SEM images of the worn flank face of the TT tool after 4-min dry cutting 45# quenched and tempered steel. It can be seen that the main wear forms of the TT tool are similar with that of the CT tool and the WCT tool. However, the abrasive wear at the flank face of the TT tool which was concentrated in the tool tip was slighter than that of the CT tool and the WCT tool. Besides, Fe, W, and C elements were detected in the selected wear area at the flank face near the main cutting edge of the TT tool through the EDX chemical composition analysis. The detected W and C elements are tool substrate material (WC+TiC+Co) which means that the scrap iron bonded in the TT tool is less than the CT tool and the WCT tool.

Panels a and b in Fig. 17 show the SEM images of the worn flank face of the WTT tool after 4-min dry cutting 45# quenched and tempered steel. It can be seen that the main wear forms of the WTT tool are similar with that of the former three tools. However, the wear condition at the flank face of the WTT tool was obviously slighter than that of the other three tools. Besides, Fe, W, S, and Zr elements were detected in the selected wear area at the flank face near the main cutting edge of the TT tool through the EDX chemical composition analysis. Due to dual functions of Micro-Nano texture and WS_2 soft coating, the friction and wear of tool-workpiece take place in the coating transfer film, and that results in significant decrease of the flank wear of the WTT tool and the adhesion of the workpiece. Seemingly, WTT tool demonstrates the best anti-adhesion and wear-resistance properties on the flank face among all the tools tested under the same cutting conditions.

According to the above research, it is found that the WTT tool

shows the best anti-adhesion and wear-resistance properties among all the tools tested under the same cutting conditions, whether on the rake face or on the flank face.

Fig. 18 illustrates the worn width *VB* at the flank face of the CT, WCT, TT, and WTT tools at different cutting distances when dry cutting 45# quenched and tempered steel (v = 150 m/min, f = 0.1 mm/r, a_p = 0.3 mm). It can be seen from Fig. 18 that the worn width *VB* at the flank face of the CT, WCT, TT, and WTT tools constantly increases with the increase of the cutting distance. Meanwhile, the worn width *VB* at the flank face of the WTT tool is the smallest among all the tools tested under the same cutting distance. At the beginning of the experiment, the worn width *VB* at the flank face of the WCT, TT, and WTT tools are obviously smaller than that of the CT tool. With the increase of the cutting distance, the worn width *VB* at the flank face of the TT tool and the WCT tool start to grow rapidly and approach the worn width *VB* at the flank face of the CT tool. The reason is that the effects of Micro-Nano textures and WS_2 soft coating begin to gradually fail. However, the worn width *VB* at the flank face of the WTT tool raises slowly and it is significantly smaller than that of the other three tools. When the cutting distance reaches 1800 m, the worn width *VB* at the flank face of the WTT tool is reduced by 34% compared with that of the CT tool. There are two reasons for this. Firstly, Micro-Nano textures on the flank face of the WTT tool reduce the workpiece-tool direct contact area. Secondly, WS_2 soft coating greatly reduces the average shear stress on the flank face of the WTT tool for its extremely low shear strength. This dual functions of Micro-Nano texture and WS_2 soft coating eventually lead to significant reduction of the friction between the flank face of the WTT tool and the machined surface of the workpiece. Nonetheless, when cutting distance exceeds 1800 m (the worn width *VB* at the flank face of the WTT tool reaches 0.135 mm), the worn width *VB* at the flank face of the WTT tool increases sharply. It may be because that the increased wear of WS_2 soft coating and Micro-Nano textures which leads to the gradual failure of the anti-adhesion and wear-resistance ability of the WTT tool.

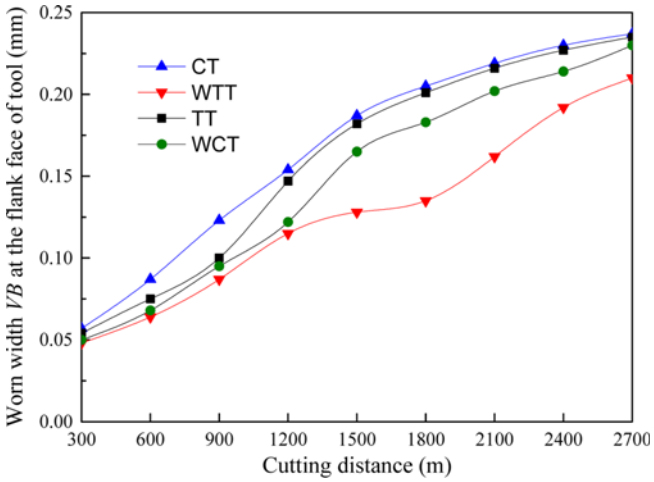

Fig. 18 Worn width *VB* at the flank face of the CT, WCT, TT, and WTT tools at different cutting distances when dry cutting 45# quenched and tempered steel (v = 150 m/min, f = 0.1 mm/r, a_p = 0.3 mm)

3.6 Machined Surface Roughness

Fig. 19 illustrates the machined surface roughness R_a when dry cutting 45# quenched and tempered steel with the CT, WCT, TT, and WTT tools at different cutting speeds (f = 0.1 mm/r, a_p = 0.3 mm). It can be seen from Fig. 19 that the the machined surface roughness R_a of the CT, TT, and WTT tools first increases and then decreases with the increase of the cutting speed. This is because the built-up edge is the main factor that affects the machined surface roughness. In a relatively high cutting speed (>150 m/min) or low cutting speed (<50 m/min) of dry cutting 45# quenched and tempered steel, the built-up edge doesn't occur at the tool nose, and the cutting-edge profile is good while the machined surface roughness is small. However, in a relatively medium cutting speed (50~150 m/min) of dry cutting 45# quenched and tempered steel, the built-up edge is easy to generate at the tool nose and the profile of the built-up edge is an irregular shape which is different with the profile of the tool nose. In addition, the profile of the built-up edge will change over time and lead to a large surface roughness.

Furthermore, from Fig. 19 we can find that the machined surface roughness R_a of WCT, TT, and WTT tools are reduced by 20~30%, 15~34%, and 32~37%, respectively, when compared with that of the CT tool under the same cutting speed. Meanwhile, WTT tool shows the smallest machined surface roughness R_a among all the tools tested under the same cutting speed. This is because that the friction and wear between the machined workpiece surface and the tool flank face is another important factor that affects the machined surface roughness. WTT tool shows the best anti-adhesion and wear-resistance properties on the flank face and good lubricity with the WS_2 soft coating. Therefore, the friction between WTT tool flank face and the machined workpiece surface reduces much, and consequently, the machined surface roughness reduces much as well.

3.7 Mechanisms

In the cutting process, the three cutting force components (F_x, F_y, F_z) can be calculated based on the following formula:[31]

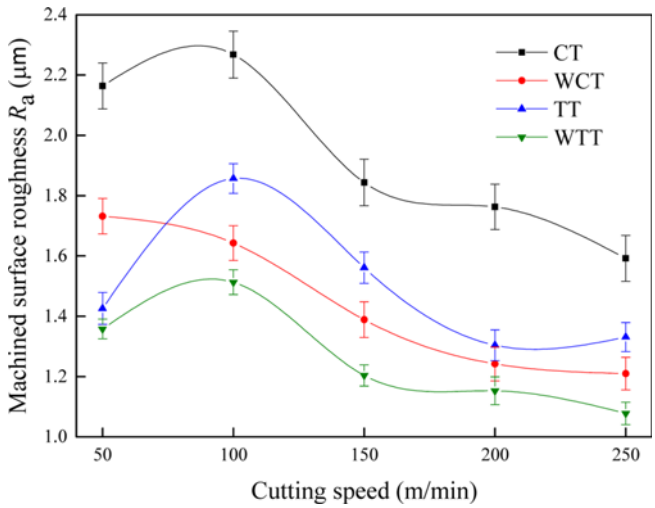

Fig. 19 Machined surface roughness R_a when dry cutting 45# quenched and tempered steel with the CT, WCT, TT, and WTT tools at different cutting speeds (f = 0.1 mm/r, a_p = 0.3 mm)

$$F_x = a_w l_f \bar{\tau}_c \left(\cos\gamma_o - \frac{\sin\gamma_o}{tg\beta}\right)\cos(\psi_r + \psi_\lambda) \quad (5)$$

$$F_y = a_w l_f \bar{\tau}_c \left(\cos\gamma_o - \frac{\sin\gamma_o}{tg\beta}\right)\sin(\psi_r + \psi_\lambda) \quad (6)$$

$$F_z = a_w l_f \bar{\tau}_c \left(\sin\gamma_o - \frac{\cos\gamma_o}{tg\beta}\right) \quad (7)$$

where a_w is the cutting width, l_f is the nominal tool-chip contact length, $\bar{\tau}_c$ is the average shear strength at the tool-chip interface, β is the friction angle, γ_o is the rake angle, ψ_r is the approach angle, and ψ_λ is the chip flow angle.

The main sources of the cutting heat during the cutting experiment are chip deformation work and friction work on the rake face and the flank face of the cutting tool. Meanwhile, a large amount of cutting heat will lead to an increase in the cutting temperature. The cutting temperature generally refers to the average temperature at the tool-chip interface on the rake face of cutting tool. The average temperature at the tool-chip interface on the rake face of cutting tool can be approximated as the sum of the average temperature at the shear plane and the friction temperature at the tool-chip interface:[32]

$$\bar{\theta}_t = \bar{\theta}_s + \bar{\theta}_f = \frac{R_1 v_s \tau_s}{c_1 \rho_1 v \sin\phi} + \theta_0 + 0.754 R_2 \bar{\tau}_c \sqrt{\frac{v l_f}{\xi c_2 \rho_2 k_2}} \quad (8)$$

where $\bar{\theta}_t$ is the average temperature at the tool-chip interface on the rake face of the cutting tool, $\bar{\theta}_s$ is the average temperature at the shear plane, $\bar{\theta}_f$ is the friction temperature at the tool-chip interface, θ_0 is the ambient temperature, R_1 is the ratio of the heat generated at the shear plane and transferred into the chip, R_2 is the ratio of the heat generated at the rake face and transferred into the chip, v_s is the shear speed, τ_s is the shear strength of the workpiece material, c_1 is the specific heat capacity of workpiece material at the average temperature $\theta_0 \sim \theta_s$, c_2 is the specific heat capacity of chip at the temperature of $(\bar{\theta}_s + \bar{\theta}_f)$, ρ_1 is the density of workpiece material, ρ_2 is the density of chip at the temperature of $(\bar{\theta}_s + \bar{\theta}_f)$, k_2 is the thermal conductivity of chip at the temperature of $(\bar{\theta}_s + \bar{\theta}_f)$. The principle of heat distribution in the cutting process is shown as Fig. 20.

Fig. 21 shows the cutting schematic of the WTT tool. In the experiment, Micro-Nano textures and WS_2 soft coating were fabricated at the tool-chip contact area of WTT tool. The actual tool-chip contact length $l_{f'}$ can be calculated as:

$$l_{f'} = l_f - n l_o = l_f - \frac{l_f}{l} l_o = \left(1 - \frac{l_o}{l}\right) l_f \quad (9)$$

where $l_{f'}$ is the actual tool-chip contact length, l_f is the nominal tool-chip contact length, n is the number of WS_2 soft coated Micro-Nano textures at the tool-chip contact area, l_o is the texture width of WS_2 soft coated Micro-Nano textures, l is the texture period of WS_2 soft coated Micro-Nano textures. From the experiment we can obtain that the texture period of WS_2 soft coated Micro-Nano textures l is 673 nm and the texture width of WS_2 soft coated Micro-Nano textures l_o is 334 nm. Therefore, the Eq. 9 can be simplified as:

$$l_{f'} = \frac{339}{673} l_f \quad (10)$$

The nominal tool-chip contact length l_f of CT tool and WTT tool are 565 μm and 497 μm, respectively, as shown in Figs. 10 and 13. The actual tool-chip contact length of CT tool is the same as the nominal tool-chip contact length of CT tool (565 μm). According to the Eq. 10, the actual tool-chip contact length $l_{f'}$ of WTT tool is 250 μm, which is 56% lower than the actual tool-chip contact length of CT tool. According to the Eq. 5-7, 10, the value of three cutting force components (F_x, F_y, F_z) are proportional to the actual tool-chip contact length $l_{f'}$. Therefore, WTT tool can significantly reduce the cutting forces when compared with CT tool. Moreover, according to the Eq. 8, under the condition that the other parameters are kept constant, the average temperature at the tool-chip interface on the rake face of cutting tool $\bar{\theta}_t$ is directly related to the square root of the nominal tool-chip contact length $\sqrt{l_f}$, which means that as $\sqrt{l_f}$ decreases, $\bar{\theta}_t$ also decreases. It can therefore be established that the WTT tool can significantly reduce the cutting temperature in comparison to the CT tool.

Besides, according to the Eqs. 5-8, the values of three cutting force components (F_x, F_y, F_z) and the average temperature at the tool-chip interface on the rake face of the cutting tool $\bar{\theta}_t$ are directly related to the average shear strength at the tool-chip interface $\bar{\tau}_t$. However, the WS_2 soft coating deposited on the surface of WTT tool has a lamellar structure with ultralow shear strength (~20 MPa) which is far less than the shear strength of the tool substrate material (700~800 MPa). As a result, the WTT tool in comparison to the CT tool can significantly reduce the cutting forces and the cutting temperature.

Fig. 22 shows the SEM image of the worn rake face of the WTT tool after 2-min dry cutting 45# quenched and tempered steel and the EDS distribution of Fe, S, and Zr elements (v = 150 m/min, f = 0.1 mm/r, a_p = 0.3 mm). It can be seen from Fig. 22 that some iron filings stick on the tool nose and the chip flow direction of the WTT tool. However, the entire rake face of the WTT tool was still covered with S and Zr elements.

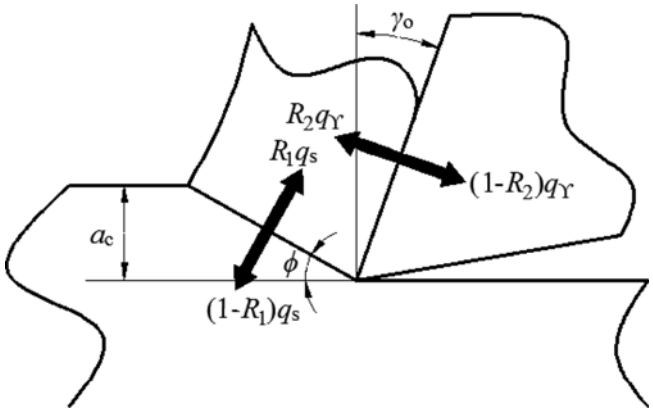

Fig. 20 Principle of heat distribution in cutting process

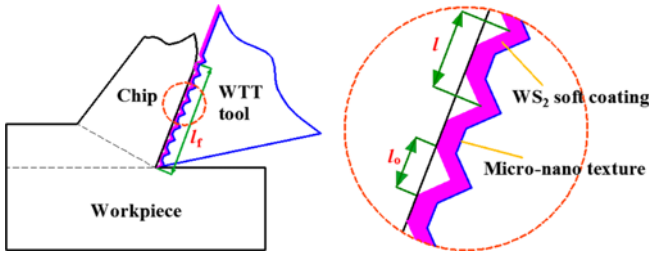

Fig. 21 Cutting schematic of WTT tool

It can be concluded from Fig. 22 that the entire tool-chip contact area of the WTT tool was still covered with WS_2 soft coating after 2-min dry cutting 45# quenched and tempered steel (v = 150 m/min, f = 0.1 mm/r, a_p = 0.3 mm). The self-lubricating mechanism of the WTT tool can be analyzed that the Micro-Nano textures on the surface of the WTT tool play a role in the storage of WS_2 soft coating. During the cutting process, a thin lubricating film is formed on the surface of the Micro-Nano textures by squeezing and dragging WS_2 soft coating, as shown in Fig. 13(b). The formation of the lubricating film can effectively reduce the adhesion and the wear of the tool. Meanwhile, the presence of Micro-Nano textures reduces the tool-chip contact area. The WS_2 soft coating on the surface of the WTT tool will be squeezed into the grooves of the Micro-Nano textures which makes the WS_2 soft coating not easy to be taken away by the chip in the cutting process. When the lubricating film is lost or ruptured, the WS_2 soft coating in the grooves of the Micro-Nano textures will be spilled from the grooves to the surface of the WTT tool due to the effects of high pressure and high temperature. Following that, the lubricating film is reformed again and again until the WS_2 soft coating is completely depleted, as shown in Fig. 23. When compared to the WTT tool, the tool chip contact area of the WCT tool is larger and the WS_2 soft coating without Micro-Nano textures is easier to be taken away by the chip. Meanwhile, the loss of the WS_2 soft coating on the WCT tool is serious and will produce massive iron filings bonding, as shown in Fig. 11. Therefore, the WTT tool can effectively improve the anti-adhesion and wear-resistance properties and increase the tool life.

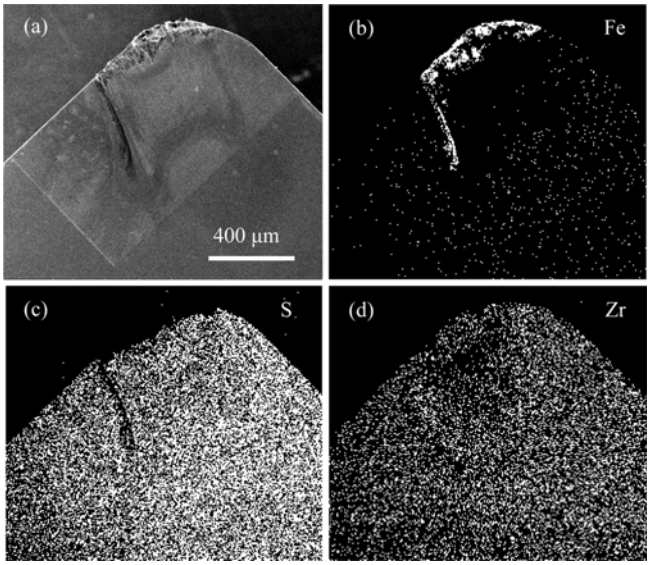

Fig. 22 SEM image of the worn rake face of the WTT tool after 2-min dry cutting 45# quenched and tempered steel and the EDS distribution of Fe, S, and Zr elements (v = 150 m/min, f = 0.1 mm/r, a_p = 0.3 mm)

4. Conclusions

To conclude, we have formed a new dry cutting tool called WS_2 soft coated Micro-Nano textured self-lubricating dry cutting tool. In this paper, we report on the dry turning tests on 45# quenched and tempered steel with WS_2 soft coated Micro-Nano textured self-lubricating dry cutting tool and other three kinds of alternative tools. The machining performance was assessed in terms of the cutting forces, cutting temperature, friction coefficient at the tool-chip interface, chip deformation, tool wear, and surface roughness of the machined workpiece. Through theoretical analysis and experimental results, the mechanisms of the WS_2 soft coated Micro-Nano textured self-lubricating dry cutting tool in improving cutting performance were put forward. The main conclusions obtained can be summarized as follows.

Three cutting force components of WCT, TT, and WTT tools are reduced by 9~31%, 8~18%, and 10~44%, respectively, when compared with those of the CT tool. Besides, WTT tool shows the smallest cutting forces among all the tools tested under the same cutting conditions, especially in relatively high-speed conditions.

The cutting temperature of WCT, TT, and WTT tools are reduced by 10~12%, 8~9%, and 12~16%, respectively, when compared with that of the CT tool. Among all the tools tested, the WTT tool shows the smallest cutting temperature under the same cutting conditions, especially in relatively high-speed conditions.

The WTT tool demonstrates the smallest average friction coefficient at the tool-chip interface and the smallest chip deformation coefficient among all the tools tested under the exact same cutting conditions.

WTT tool shows the best anti-adhesion and wear-resistance properties among all the tools tested under the same cutting conditions, whether on the rake face or on the flank face. From the contrast tests of cutting wear process, we can find that the worn width *VB* at the flank face of the CT tool and the WTT tool constantly increases with the increase of cutting distance. Meanwhile, the worn width *VB* at the flank face of the WTT tool are smaller than that of the CT tool under the same cutting distance.

The effect of Micro-Nano texture and WS_2 soft coating on the cutting forces and the cutting temperature is analyzed. Micro-Nano texture can reduce the actual tool-chip contact length and WS_2 soft coating can reduce the average shear strength at the tool-chip interface. Micro-Nano texture and WS_2 soft coating both can significantly reduce the cutting forces and the cutting temperature. Besides, the self-lubricating mechanism of the WTT tool is revealed. The Micro-Nano

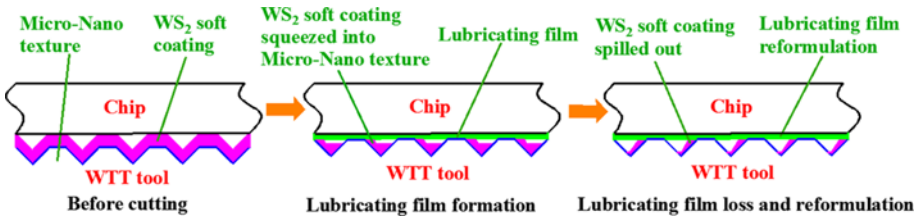

Fig. 23 Self-lubricating mechanism of WTT tool in cutting process

textures on the surface of the WTT tool play a role in the storage of WS_2 soft coating. During the cutting process, a thin lubricating film is formed on the surface of the Micro-Nano textures by squeezing and dragging WS_2 soft coating. When the lubricating film is lost or ruptured, the WS_2 soft coating in the grooves of the Micro-Nano textures will be spilled from the grooves to the surface of the WTT tool due to the effects of high pressure and high temperature. Then, the lubricating film is reformed again and again until the WS_2 soft coating is completely depleted. Therefore, the WTT tool can effectively improve the anti-adhesion and wear-resistance properties and increase the tool life.

ACKNOWLEDGEMENT

This work was supported by the National Natural Science Foundation of China (Grant No. 51505399), Natural Science Foundation of Fujian Province of China (Grant No. 2017J05088), and Joint Innovation of Industrial Technology in Fujian Province in 2016 (Serial development of CNC tools precision and high efficiency processing titanium alloy, Fujian Province Development and Reform Commission Investment No. [2016] 482).

REFERENCES

1. Wiklund, U., Rubino, S., Kádas, K., Skorodumova, N. V., Eriksson, O., et al., "Experimental and Theoretical Studies on Stainless Steel Transfer onto a TiN-Coated Cutting Tool," Acta Materialia, Vol. 59, No. 1, pp. 68-74, 2011.
2. Deng, J. X., Song, W. L., and Zhang, H., "Design, Fabrication and Properties of a Self-Lubricated Tool in Dry Cutting," International Journal of Machine Tools and Manufacture, Vol. 49, No. 1, pp. 66-72, 2009.
3. Liu, Z. F., Zhang, C. G., and Ren, J. L., "Dry Machining Technology and Application," China Machine Press, 2005.
4. Faga, M. G., Priarone, P. C., Robiglio, M., Settineri, L., and Tebaldo, V., "Technological and Sustainsaility Implications of Dry, Near-Dry, and Wet Turning of Ti-6Al-4V Alloy," Int. J. Precis. Eng. Manuf.-Green Tech., Vol. 4, No. 2, pp. 129-139, 2017.
5. Zhao, J., Ai, X., and Lu, Z. J., "Preparation and Characterizaion of Si_3N_4/TiC Nanocomposite Ceramics," Materials Letters, Vol. 60, No. 23, pp. 2810-2813, 2006.
6. Loginov, P., Jr, L. M., Levashov, E.. and Petrzhik, M., "Diamond and CBN Hybrid and Nanomodified Cutting Tools with Enhanced Performance: Development, Testing and Modelling," Materials & Design, Vol. 88, pp. 310-319, 2015.
7. Dureja, J. S., Singh, R., Singh, T., Singh, P., Dogra, M., et al., "Performance Evaluation of Coated Carbide Tool in Machining of Stainless Steel (AISI 202) under Minimum Quantity Lubrication (MQL)," Int. J. Precis. Eng. Manuf.-Green Tech., Vol. 2, No. 2, pp. 123-129, 2015.
8. Michailidis, M., "Variations in the Cutting Performance of PVD-Coated Tools in Milling Ti6Al4V, Explained Through Temperature-Dependent Coating Properties," Surface and Coatings Technology, Vol. 304, pp. 325-329, 2016.
9. Broniszewski, K., Wozniak, J., Kostecki, M., Czechowski, K., Jaworska, L., et al., "Al_2O_3-V Cutting Tools for Machining Hardened Stainless Steel," Ceramics International, Vol. 41, No. 10, pp. 14190-14196, 2015.
10. Deng, J. X., Cao, T. K., and Yang, X. F., "Self Lubrication of Sintered Ceramic Tools with CaF_2 Additions in Dry Cutting," International Journal of Machine Tools and Manufacture, Vol. 46, No. 9, pp. 957-963, 2006.
11. Olofinjana, B., Martin, C. L., Ajayi, O. O., and Ajayi, E. O., "Effect of Laser Surface Texturing (LST) on Tribochemical Films Dynamics and Friction and Wear Performance," Wear, Vol. 332-333, pp. 1225-1230, 2015.
12. Chen, P., Xiang, X., Shao, T., La, Y., and Li, J., "Effect of Triangular Texture on the Tribological Performance of Die Steel with TiN Coatings under Lubricated Sliding Condition," Applied Surface Science, Vol. 389, pp. 361-368, 2016.
13. Li, J., He, Y., Xiong, D., Qin, Y., Chen, J., et al., "Tribological Properties of Silver Coatings with Laser Surface Textured Nickel as Interlayer," Tribology International, Vol. 100, pp. 178-185, 2016.
14. Xu, Y., Peng, Y., Dearn, K. D., You, T., Geng, J., et al., "Fabrication and Tribological Characterization of Laser Textured Boron Cast Iron Surfaces," Surface and Coatings Technology, Vol. 313, pp. 391-401, 2017.
15. Kovalchenko, A., Ajayi, O., Erdemir, A., and Fenske, G., "Friction and Wear Behavior of Laser Textured Surface Under Lubricated Initial Point Contact," Wear, Vol. 271, Nos. 9-10, pp. 1719-1725, 2011.
16. Lei, S., Devarajan, S., and Chang, Z. H., "A Study of Micropool Lubricated Cutting Tool in Machining of Mild Steel," Journal of Materials Processing Technology, Vol. 209, No. 3, pp. 1612-1620, 2009.
17. Sharma, V. and Pandey, P. M., "Recent Advances in Turning with Textured Cutting Tools: A Review," Journal of Cleaner Production, Vol. 137, pp. 701-715, 2016.
18. Sugihara, T. and Enomoto, T., "Development of A Cutting Tool with A Nano/Micro-Textured Surface-Improvement of Anti-Adhesive Effect by Considering the Texture Patterns," Precision Engineering, Vol. 33, No. 4, pp. 425-429, 2009.
19. Arulkirubakaran, D., Senthilkumar, V., and Kumawat, V., "Effect of Micro-Textured Tools on Machining of Ti-6Al-4V Alloy: An Experimental and Numerical Approach," International Journal of Refractory Metals and Hard Materials, Vol. 54, pp. 165-177, 2016.
20. Koshy, P. and Tovey, J., "Performance of Electrical Discharge Textured Cutting Tools," CIRP Annals-Manufacturing Technology, Vol. 60, No. 1, pp. 153-156, 2011.

21. Deng, J. X., Wu, Z., Lian, Y. S., Qi, T., and Cheng, J., "Performance of Carbide Tools with Textured Rake-Face Filled with Solid Lubricants in Dry Cutting Processes," International Journal of Refractory Metals and Hard Materials, Vol. 30, No. 1, pp. 164-172, 2012.

22. Hao, R., Tedstone, A. A., Lewis, D. J., Warrens, C. P., West, K. R., et al., "Property Self-Optimization during Wear of MoS_2," ACS Applied Materials & Interfaces, Vol. 9, No. 2, pp. 1953-1958, 2017.

23. Cao, X., Shi, Y., Shi, W., Rui, X., Yan, Q., et al., "Preparation of MoS_2-Coated Three-Dimensional Graphene Networks for High-Performance Anode Material in Lithium-Ion Batteries," Small, Vol. 9, No. 20, pp. 3433-3438, 2013.

24. Zhang, X., Vitchev, R. G., Lauwerens, W., Stals, L., He, J., et al., "Effect of Crystallographic Orientation on Fretting Wear Behaviour of MoS_x Coatings in Dry and Humid Air," Thin Solid Films, Vol. 396, Nos. 1-2, pp. 69-77, 2001.

25. Scharf, T. W., Prasad, S. V., Dugger, M. T., Kotula, P. G., Goeke, R. S., et al., "Growth, Structure, and Tribological Behavior of Atomic Layer-Deposited Tungsten Disulphide Solid Lubricant Coatings with Applications to MEMS," Acta Materialia., Vol. 54, No. 18, pp. 4731-4743, 2006.

26. Wang, D., Hu, M., Jiang, D., Gao, X., Fu, Y., et al., "Preparation and Characterization of the CrN Nanocone Array Textured WS_2 Film," Materials Letters, Vol. 188, pp. 267-270, 2017.

27. Zheng, X. H., Tu, J. P., Lai, D. M., Peng, S. M., Gu, B. et al., "Microstructure and Tribological Behavior of WS_2-Ag Composite Films Deposited by RF Magnetron Sputtering," Thin Solid Films, Vol. 516, No. 16, pp. 5404-5408, 2008.

28. Zhu, L. N., Wang, C. B., Wang, H. D., Xu, B. S., Zhuang, D. M., et al., "Tribological Properties of WS_2 Composite Film Prepared by A Two-Step Method," Vacuum, Vol. 85, No. 1, pp. 16-21, 2010.

29. Aldana, P. U., Dassenoy, F., Vacher, B., Mogne, T. L., and Thiebaut, B., "WS_2 Nanoparticles Anti-Wear and Friction Reducing Properties on Rough Surfaces in the Presence of ZDDP Additive," Tribology International, Vol. 102, pp. 213-221, 2016.

30. Wang, A. H., Zhang, X. L., Zhang, X. F., Qiao, X. Y., Xu, H. G., et al., "Ni-Based Alloy/Submicron WS_2 Self-Lubricating Composite Coating Synthesized by Nd:YAG Laser Cladding," Materials Science and Engineering: A, Vol. 475, Nos. 1-2, pp. 312-318, 2008.

31. Chen, R. Y., "Principle of Metal Cutting," China Machine Press, 1992.

32. Loewen, E. and Shaw, M., "On the Analysis of Cutting Tool Temperatures," Trans. ASME, Vol. 76, pp. 217-225, 1954.